RSC Advances

PAPER

View Article Online
View Journal | View Issue

Cite this: *RSC Adv.*, 2020, **10**, 44958

A comprehensive optical and electrical study of unsymmetrical imine with four thiophene rings and their binary and ternary compositions with PTB7 and $PC_{70}BM$ towards organic photovoltaics†

Beata Jewłoszewicz,[a] Krzysztof Artur Bogdanowicz,[a] Wojciech Przybył,[a] Karolina Dysz,[a] Agnieszka Dylong,[a] Agnieszka Gonciarz,[b] Robert Pich,[b] Wojciech Mech,[c] Krzysztof P. Korona,[c] Maria Kamińska,[c] Kamila Zarębska,[d] Magdalena Skompska,[d] Andrzej Kaim,[d] Arkadiusz Ciesielski[c] and Agnieszka Iwan*[a]

A new unsymmetrical imine with four thiophene rings was synthesized in a one-step reaction, starting from the commercially available and relatively inexpensive reagents. The obtained imine in the form of thin films exhibited photoluminescence properties in the 1.8–2.4 eV energy range and a photoluminescence lifetime of about 0.3 ns. The HOMO and LUMO levels of the imine determined by cyclic voltammetry were at about −5.19 eV and −3.05 eV, respectively. The density functional theory was applied to calculate the geometric and electronic structure of the imine. The UV-Vis spectra showed that the absorption range of the imine overlaps with that of $PC_{70}BM$, and the absorption peak at the maximum of the imine at 424 nm is located between the two maxima at 404 nm and 461 nm of the fullerene derivative. The electron acceptor and donor activity of the imine was tested in the solar cell architecture: glass/ITO/PEDOT:PSS/active layer/In/Al. The best photovoltaic parameters, with very good reproducibility for each 8 pixels in the cell, were found for the active layer based on ternary mixture PTB7:$PC_{70}BM$:imine at a weight ratio 8 : 13 : 1, with the power conversion efficiency of about 4%. The external quantum efficiency of devices with the imine was found to be about 40% at 3.3 eV. The thermal imaging together with the recorded current response at increasing potential showed that the presence of imine in the composition has a beneficial impact in terms of current flow stability at temperatures above 200 °C, compared to two component layers with the same imine as an additive.

Received 1st October 2020
Accepted 25th November 2020

DOI: 10.1039/d0ra08330e

rsc.li/rsc-advances

1. Introduction

Organic (polymer) solar cells have attracted much attention over the past 50 years due to their potential in commercial applications. For this reason, a lot of organic materials with complicated chemical structure, including semiconducting polymers, small organic compounds or dendrimers, have been proposed for practical usage in various optoelectronic devices.[1–13]

Considering the polymer structure used as a donor component of active layer in the photovoltaic devices, three commercial polymers, poly(3-hexylthiophene) (P3HT), poly[*N*-9″-heptadecanyl-2,7-carbazole-*alt*-5,5-(4′,7′-di-2-thienyl-2′,1′,3′-benzothiadiazole)] (PCDTBT) and poly[[4,8-bis[(2-ethylhexyl)oxy]benzo[1,2-*b*:4,5-*b*′]dithiophene-2,6-diyl][3-fluoro-2-[(2-ethylhexyl)carbonyl]thieno[3,4-*b*]thiophenediyl]] (PTB7), have been widely investigated. As the second component of the active layer, [6,6]-phenyl-C_{61}-butyric acid methyl ester (PCBM) or [6,6]-phenyl-C_{70}-butyric acid methyl ester ($PC_{70}BM$) are mainly used as an acceptor in bulk heterojunction (BHJ) devices.[3,4,14,15]

Imines (azomethines, Schiff bases) are a well-known class of organic compounds used mainly in biology, pharmacy, medicine, optoelectronics and photonics including liquid crystals due to their electrochromic and halochromic properties.[16–25]

The highest value of power conversion efficiency (PCE) for imines was obtained for perovskite solar cells. Iwan *et al.*[26] applied with success a symmetrical imine with thiadiazole and triphenylamine units (TPA) in perovskite solar cells as the hole transporting materials and received a PCE of 14.4% without hysteresis effect. Petrus *et al.*[27] used an azomethine-based small molecule with TPA units for the hole transporting material layer

[a]*Military Institute of Engineer Technology, Obornicka 136 Str., 50-961 Wroclaw, Poland. E-mail: iwan@witi.wroc.pl*

[b]*Faculty of Security and Safety Research, General Tadeusz Kosciuszko Military University of Land Forces, Czajkowskiego 109 Str., 51-147 Wroclaw, Poland*

[c]*Faculty of Physics, University of Warsaw, Pasteura 5, 02-093 Warsaw, Poland*

[d]*Faculty of Chemistry, University of Warsaw, Pasteura 1, 02-093, Warsaw, Poland*

† Electronic supplementary information (ESI) available. See DOI: 10.1039/d0ra08330e

of a thickness of *ca.* 40 nm in perovskite solar cells with PCE 11.0%.

Unfortunately, up to now the imines in organic (polymer) solar cells have not exhibited as high efficiency as other organic compounds.[28] Even if chemical structure modifications are widely proposed and additional side chains and functional groups are incorporated into imines' structure to improve their solubility, the solar cell efficiency is still not satisfying. Our review showed that taking into consideration the components of active layers (donor and acceptor), the PCE values of organic solar cells based on imine as a donor were found in the range of 0.1–2.17%.[29–33] In ref. 33, a symmetrical imine was used as the donor component in the device ITO/MoO_x/TPA–TBT–TPA:$PC_{70}BM$ (1 : 5)/Mg/Al and the efficiency was found in the range of 1.97–2.17%, depending on the annealing time.

In ref. 29, the authors achieved PCE = 1.21% for a device with imine with TPA and thiophene moieties in the active layer with an architecture of ITO/MoO_3/TPA–N=CH–Th–CH=N–TPA:$PC_{70}BM$/LiF/Al. In ref. 31, the imines with benzodifuran moieties and thiophene rings were tested as donor materials in bilayer solar cells, where C60 was used as an acceptor and the measured PCE was 1.18%. In ref. 34, the authors investigated imines with thiophene and imide moieties in polymer solar cells with an architecture of ITO/PEDOT:PSS/imine:P3HT/Al and a PCE in the range of 0.69–0.90% was obtained.

Imines were also investigated as acceptors in the active layer of organic solar cells and a PCE in the range of 0.03–0.46% was obtained. In ref. 30, the authors recommended (5-(10-undecyloxy)-2-[[[4-hexylphenyl]imino]methyl]phenol) with liquid crystalline properties as an acceptor in the active layer with P3HT. The resulting PCE was 0.27% after annealing the active layer in the temperature of the phase transition (PCE before annealing was 0.16%).

In ref. 35, the authors investigated symmetrical and unsymmetrical imines with naphthalene moieties in polymer solar cells with an architecture of ITO/PEDOT:PSS/P3HT (or P3OT):imine/Al and the obtained PCE was in the range of 0.17–0.32%. Moreover, a series of polyaromatic hydrocarbons with anthracene, phenanthrene and pyrene units connected with imine were investigated in polymer solar cells as the acceptor component in the devices with an architecture of ITO/PEDOT:PSS/P3HT (or P3OT):imine/Al and PCE in the range of 0.03–0.21% was obtained.[36]

It is well known that ternary active layers are very promising for organic solar cells.[37] For this reason, azomethine naphthalene diimides were used as the components of binary (P3HT:imine) and ternary (P3HT:PCBM:imine) active layers in bulk heterojunction solar cells.[38] The efficiency of the solar cell with a binary active layer was rather low (0.46%) in comparison with that of the reference device based on P3HT:PCBM (PCE = 3.88%), while the PCE of the cell with a ternary active layer was in the range of 0.24–5.50%, depending on the chemical structure of the imine used.

In our previous work, we investigated symmetrical and unsymmetrical imines with thiophene and thiazole moieties as the component of ternary active layer in organic solar cells with an architecture of ITO/PEDOT:PSS/PTB7:imine:$PC_{70}BM$/Al and we reached PCE = 0.42%.[39]

Our scientific review has shown that there is still little research on the application of imines in photovoltaics, and in particular, there is no clear answer why, despite being well-suited, the imines are not efficient compounds in photovoltaic devices. Imines are also attractive for green energy since they can be synthesized in a one-step condensation reaction of aldehyde/dialdehyde and amines/diamines in the solution or solid state with only water as a co-product of the reaction.[16]

Inspired by the above-described findings, we conducted a detailed study of the structure-spectroscopic and electrical properties of a new unsymmetrical imine (PV-BLJ-SC9) synthesized from 4-(thiophene-3-yl)aniline and 2,2′:5′,2″-terthiophene-5-carboxaldehyde for applications in optoelectronics and photonics. The selected imine properties were also tuned by supramolecular engineering *via* the creation of hybrid compositions with PTB7 and $PC_{70}BM$, or both of them. Various devices based on the imine were constructed, and their electrical properties (photovoltaics and IR thermal) were investigated, taking into account three factors:

- type of active layer,
- concentration of imine in active layer,
- time stability in air atmosphere.

The optical properties such as absorption, normal reflection and transmission together with the photoluminescence of the imine and binary and ternary compositions were investigated in detail to optimize the ratio of imine to PTB7:$PC_{70}BM$ for photovoltaic application. Compared with our previous results,[39] in this paper we increased the efficiency of the polymer solar cells based on PTB7:$PC_{70}BM$:imine from 0.42 to 4.0% as a result of incorporating a new synthesised unsymmetrical imine with four thiophene rings.

2. Experimental

2.1. Materials

All chemicals and solvents for the imine synthesis were of reagent grade and were obtained from Aldrich Chemical Co (Saint Louis, MO, USA). The most important ingredients for solar cell construction: poly[[4,8-bis[(2-ethylhexyl)oxy]benzo[1,2-*b*:4,5-*b*′]dithiophene-2,6-diyl][3-fluoro-2-[(2-ethylhexyl)carbonyl]thieno[3,4-*b*]thiophenediyl]] (PTB7) (M215 butch), [6,6]-phenyl-C_{70}-butyric acid methyl ester ($PC_{70}BM$), poly(3,4-ethylenedioxythiophene) polystyrene sulfonate (PEDOT:PSS) (Heraeus Clevios AI 4083), and indium tin oxide (ITO) 8 pixel glass substrates were purchased from Ossila. Solvents for active layer preparation: chlorobenzene (CB) and 1,8-diiodooctane (DIO) were purchased from Sigma-Aldrich.

2.1.1. Organic solar cells preparation. Active layer solutions were prepared in Ar atmosphere a day before solar cell construction. A reference solution of PTB7:$PC_{70}BM$ with a weight ratio 2 : 3 was prepared in 97% chlorobenzene with 3% of DIO at a concentration of 25 mg mL^{-1}, then stirred for 24 h at 50 °C, and filtered through a 0.45 μm PTFE syringe filter. Pure PV-BLJ-SC9 solution was prepared in chlorobenzene also at 25 mg mL^{-1} concentration, stirred for 24 h at 50 °C, and used without filtration. Binary solutions of PTB7:PV-BLJ-SC9 and PV-BLJ-SC9:$PC_{70}BM$ in chlorobenzene were prepared at 2 : 3 weight ratio at 25 mg mL^{-1} concentration. Firstly, pure PTB7 (10 mg

mL^{-1}) and $PC_{70}BM$ (15 mg mL^{-1}) solutions were prepared and stirred for 2 h at 50 °C, then filtered through a 0.45 μm PTFE syringe filter. Filtered solutions were then poured into the solution of PV-BLJ-SC9 to create a target concentration of 25 mg mL^{-1}, stirred for 24 h at 50 °C and used without filtration. Ternary mixtures of (PTB7:PV-BLJ-SC9):$PC_{70}BM$ were prepared in chlorobenzene containing 3% of DIO at 25 mg mL^{-1} concentration and weight ratios of (4 : 1) : 8 or (8 : 1) : 13. At first, PTB7:$PC_{70}BM$ solutions (7.7 mg mL^{-1} : 15 mg mL^{-1} or 9 mg mL^{-1} : 15 mg mL^{-1}) were stirred for 2 h at 50 °C, and then filtered through 0.45 μm PTFE syringe filter. Filtered solutions were poured into PV-BLJ-SC9 to create target concentrations, then stirred for 24 h at 50 °C and used without further filtration.

Solar cells were fabricated on ITO-coated glass substrates in Ar atmosphere, with an architecture of ITO/PEDOT:PSS/active layer/Al. The substrates had 8 separated pixels giving the single cell area of 4 mm^2 per each pixel. The active layer was either PV-BLJ-SC9 imine alone or its blends with PTB7 and/or $PC_{70}BM$. In a reference cell, the active layer was in the form of a PTB7:$PC_{70}BM$ bulk heterojunction (BHJ), where PTB7 and $PC_{70}BM$ were used as donor and acceptor materials, respectively. In (PTB7:PV-BLJ-SC9):$PC_{70}BM$ ternary mixtures, PV-BLJ-SC9 imine was used as an additive to the PTB7 donor, replacing 1/5 or 1/9 of it. In binary BHJ mixtures of PTB7:PV-BLJ-SC9 or PV-BLJ-SC9:$PC_{70}BM$, the PV-BLJ-SC9 imine was used as the donor or acceptor material, respectively, replacing the PTB7 donor or $PC_{70}BM$ acceptor materials in the reference active layer of PTB7:$PC_{70}BM$.

First, the surface of ITO-coated glass substrates was cleaned with deionised water, dried with compressed nitrogen, and activated by 5 min treatment in an Ossila UV Ozone Cleaner. On such prepared substrates, a PEDOT:PSS layer was deposited by spin coating (5000 rpm) from PEDOT:PSS aqueous solution filtered through a 0.45 μm PES syringe filter. The obtained PEDOT:PSS film of thickness 30 nm was annealed on a hot plate at 150 °C for 15 min, and then the substrates were transferred to an Ar glove box for active layer deposition. The pre-prepared active layer solutions were spin-coated on ITO substrates with a PEDOT:PSS layer. PTB7:$PC_{70}BM$, PTB7:PV-BLJ-SC9 and (PTB7:PV-BLJ-SC9):$PC_{70}BM$ solutions were spin-coated with a rotation speed of 900 rpm for 60 s, to obtain the layers of thickness 90 nm. The solution of PV-BLJ-SC9:$PC_{70}BM$ was spin-coated with a rotation speed of 600 rpm for 60 s and a 50 nm thick layer was obtained. Pure PV-BLJ-SC9 imine solution was spin-coated with a rotation speed of 600 nm for 60 s, and in this case the thickness of the obtained layer was 100 nm. After active layer deposition, the substrates were dried for 15 min under vacuum in the glovebox antechamber. Then, aluminium and indium electrodes were deposited by thermal evaporation under vacuum of about 3×10^{-8} bar. Finally, the organic solar cells were encapsulated by a thin glass sheet and epoxy cured under UV lamp for 15 min. Devices were stored in a standard atmosphere with a reduced influx of sunlight.

2.2. Characterization methods

Cyclic voltammetry measurements (CV) were performed with a potentiostat PGSTAT 302N (Autolab, Metrohm, The Netherlands) in a standard three electrode electrochemical cell, with a Pt disc of the surface area of 0.03 cm^2 as the working electrode, a Pt wire as the counter electrode and Ag/Ag^+ (0.1 M) in acetonitrile as the reference electrode. The potential of Ag/Ag^+ electrode was calibrated *vs.* $Ag/AgCl/Cl_{aq}^-$ (3 M) using the ferrocene/ferrocenium (Fc/Fc^+) redox couple in acetonitrile.

Theoretical calculations were performed using the GAUSSIAN 16 (ref. 39 and 40) software package. The structure of the investigated imine was optimized at the hybrid density functional DFT/B3LYP level[41–43] with the 6-31G(d) basis set, to a stationary point on the Born–Oppenheimer potential energy surface proved by the absence of imaginary frequencies. The frontier HOMO and LUMO were calculated on fully optimized structures by employing both the DFT/B3LYP/6-31G(d) and PBE/6-311G(d,p)[44] approaches.

For time-resolved PL (TRPL) excitation, a mode-locked Ti:sapphire laser with frequency-tripled (to wavelength of 300 nm, 4.2 eV energy) output pulses (pulse duration 130 fs) was applied and the temporal distribution was analyzed by the Hamamatsu streak camera in time ranges of picoseconds and nanoseconds. For these measurements, the samples were drop cast (thickness ~ 1 μm) on copper substrates from chlorobenzene solution used for organic solar cell construction. Time integrated photoluminescence (PL) spectroscopy in the range of 300–900 nm was performed under the same excitation condition, using Hamamatsu C7557 CCD detector.

NIR-VIS-UV optical absorption spectra were recorded at room temperature using a Cary 5000 spectrophotometer in the range of 300–800 nm. For these measurements, the samples of mixed compositions were spin coated on glass substrates from the solutions used for organic solar cell construction and the layers of few tens of nanometers thick were studied. For pure PTB7 and $PC_{70}BM$, the solutions in chlorobenzene were prepared at 15 mg mL^{-1} concentration and spin-coated (at 900 rpm and 600 rpm, 60 s) on glass substrates, which resulted in layers of 100 nm or 50 nm thickness, respectively. In case of a sample with PV-BLJ-SC9 imine only, due to its low absorption coefficient, a drop cast deposition was applied, and the layer of about 1 μm was deposited on the glass substrate. The thickness of the layers was measured using a Dektak profilometer, so the absorption coefficients could be calculated.

The performance of bulk heterojunction (BHJ) polymer solar cells was checked by *J–V* (current density–voltage) characteristics and photo-electric spectroscopy. The *J–V* curves were measured using a Keithley 2400 Series SMU, Keithley Kick Start software and Ossila 8 pixel test board under AM1.5 solar illumination. The illumination source was a Newport VeraSol-2 LED Class AAA Solar Simulator of 1000 W m^{-2} power output.

The photo-electric spectroscopy was performed in the range of 300–1400 nm, with the use of a tungsten lamp and 0.5 meter monochromator. The photo-excited current was measured with a Keithley logarithmic pico-amperometer. The excitation intensity value that was necessary for external quantum efficiency (EQE) calculation was controlled by a calibrated power meter PM320. The excitation density was 100 μW cm^{-2}.

Thermal behaviour was observed as described elsewhere:[45] a thermographic camera (VIGOcam v50, VIGO System S.A.,

Ożarów Mazowiecki, Poland) and a multichannel potentiostat-galvanostat (PGStat Autolab M101, Metrohm, Barendrecht, The Netherlands) were used in this study.

Normal reflection spectra were collected using a F3-UV spectrometer from Filmetrics in the 250–1000 nm range. Normal transmission spectra were collected using METASH UV-6000 Spectrophotometer in the same wavelength range. The presented reflection and transmission curves are a result of averaging several recorded reflection and transmission spectra. For normal reflection and transmission experiments, the samples were prepared as follows. PV-BLJ-SC9, PTB7 and $PC_{70}BM$ in various mass ratios were suspended in chlorobenzene and left for at least 8 hours under stirring. Then, the suspension was filtered using a PTFE filter with 0.45 μm pore size and spin-cast onto glass substrates rotating at 900 rpm. In the case of samples comprising PTB7 and $PC_{70}BM$, the thickness of resultant films was in the range of 80–90 nm. In the case of pure PV-BLJ-SC9, the thickness was hard to estimate, since the adhesion of the pure imine to glass is very low. Therefore, the thickness of the PV-BLJ-SC9 layer varied from spot to spot, and thus the reflection and transmission results for the pure imine are only qualitative.

3. Results and discussion

The synthesis and characterization of imine PV-BLJ-SC9 is presented in the ESI.† In-depth ^{1}H NMR analysis showed that the result of the synthesis was a mixture of *cis* and *trans* isomers as we observe two singlets located close to each other (approx. 8.54 ppm). The simulated ^{1}H NMR spectra presented in the ESI (Fig. S1)† also contained two signals at 8.50 ppm and 8.75 ppm for *trans*-PV-BLJ-SC9 and *cis*-PV-BLJ-SC9, respectively. However, the separation of these stable isomers was impossible due to the low solubility of the synthesized imine in most conventional solvents. Therefore, the obtained mixture was subjected to further investigations without determining the ratio of both isomers. The chemical structure of *trans*-PV-BLJ-SC9 and *cis*-PV-BLJ-SC9 imine together with a model of HOMO and LUMO orbitals for both optimized isomer molecules, discussed further in the text, are shown in Scheme 1.

Theoretical calculations show that Hartree–Fock energies of the *trans* and *cis* isomers of PV-BLJ-SC9 differ very little by 0.01 eV. This means that both isomers are almost equally stable from the thermodynamic point of view (the *trans* structure is more stable by 0.01 eV). Both isomers cannot transform into each other due to the fact that it would have to break the –HC=N– double bond. Their concentrations are determined by the condensation mechanism during which this imine is formed. The possibility of occurrence of both PV-BLJ-SC9 isomers is obviously confirmed by experimental and theoretical ^{1}H NMR spectra.

In order to select the most suitable solvent for the electrochemical, optical and photovoltaic investigations of PV-BLJ-SC9, the solubility of imine was tested by placing 1.0 mg into a vial containing 1 mL of the solvent and subsequently ultrasonicated for 15 min. After this time, the vials were put aside for about 15 minutes and observations were noted down. The

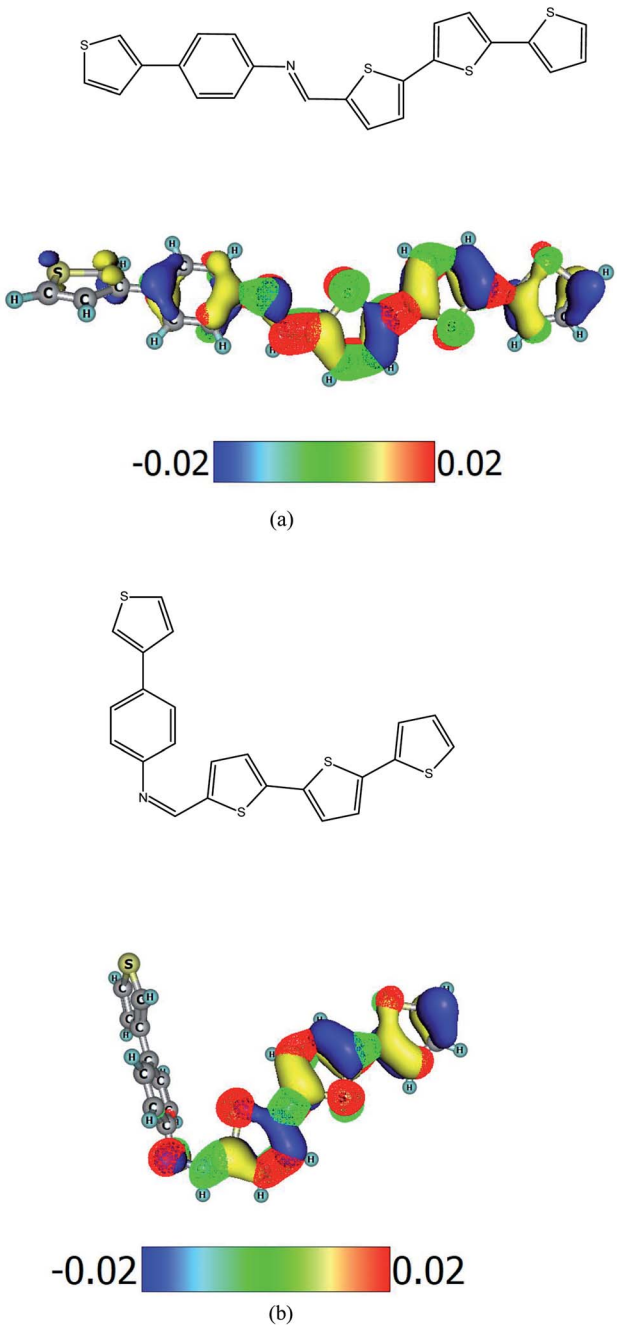

Scheme 1 Chemical structure of *trans*-PV-BLJ-SC9 (a) and *cis*-PV-BLJ-SC9 (b) along with modeled HOMO (blue and yellow) and LUMO (red and green) orbitals for optimized PV-BLJ-SC9 molecule. Red and yellow lobes correspond to positive whereas blue and green lobes to negative isosurface values.

results of solubility tests in the selected solvents for PV-BLJ-SC9 after addition of 1 mL of solvent are as follows, in decreasing order: dichloroethane > dichloromethane > dichlorobenzene > acetone > *o*-xylene > *n*-heptane > isopropanol ethanol > methanol (see Fig. S1†). For *n*-heptane and other alcohols, an undissolved solid was observed in the vial even after addition of another 1 mL of the solvent. The best group of solvents were chlorinated compounds, hence they were used for further

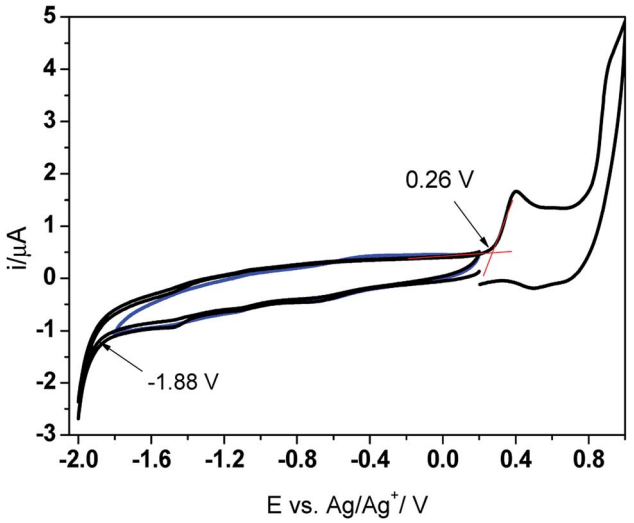

Fig. 1 Cyclic voltammograms obtained on a Pt electrode in dichloromethane (DCM) containing PV-BLJ-SC9 and 0.1 M $TBAPF_6$ supporting electrolyte.

studies, taking also into account the solubility of poly[[4,8-bis[(2-ethylhexyl)oxy]benzo[1,2-*b*:4,5-*b*′]dithiophene-2,6-diyl][3-fluoro-2-[(2-ethylhexyl)carbonyl]thieno[3,4-*b*]thiophenediyl]] (PTB7).

3.1. Electrochemical properties of imine

The new imine was studied by cyclic voltammetry (CV) to determine the HOMO–LUMO levels and the band gap energy. The PV-BLJ-SC9 was dissolved in dichloromethane (3.2 mg in 25 mL DCM) containing 0.1 M $TBAPF_6$ as the supporting electrolyte. The cyclic voltammograms were recorded on a Pt electrode at the scan rate of 100 mV s^{-1} in the standard electrochemical cell, containing a Ag/Ag^+ (0.1 M $AgNO_3$ in acetonitrile) reference electrode and Pt wire as the counter electrode. Prior to the experiments, the solution was deaerated by bubbling with Ar. The energies of HOMO and LUMO levels were determined from the onset potentials for reduction (E^{red}_{onset}) and oxidation (E^{ox}_{onset}), respectively, in the first scan recorded in the potential range 0.2 → −2.0 → 1.0 V. In order to refer the HOMO and LUMO levels to the energetic vacuum scale, the onset potentials were related to the standard hydrogen electrode (SHE), assuming that the potential of the Ag/Ag^+ reference electrode is 0.505 V *vs.* SHE. Then, the E_{HOMO} and E_{LUMO} were determined from the equations:

$$E_{LUMO} = -(E^{red}_{onset} + 4.44)\ eV$$

$$E_{HOMO} = -(E^{ox}_{onset} + 4.44)\ eV$$

Based on the results presented in Fig. 1, the energies of the HOMO and LUMO levels were calculated at about −5.20 eV and −3.06 eV, respectively. Thus, the electrochemical band gap energy (E^{el}_g) is 2.14 eV. This value is in very good agreement with the optical band gap energy (E^{opt}_g = 2.48 eV) determined from the absorbance onset in the UV-Vis spectrum of PV-BLJ-SC9 dissolved in DCM (Fig. 4).

It is interesting to note that in the first cyclic voltammogram performed in the imine solution, there are two oxidation peaks at about 0.4 V and 0.85 V. Since the imine contains thiophene units at both ends of the molecule, the less positive peak probably corresponds to oxidation of the thiophene from the three-thiophene block, while the single thiophene is oxidized at the higher potential. When the Pt electrode was cycled several times in the imine solution in the potential range from −0.5 V to 1.0 V, one can observe the evident features of electropolymerization, *i.e.* development of two new oxidation peaks (A and B) and their reduction counterparts (A′ and B′, respectively) (Fig. 2a). The intensity of both redox couples gradually increases in the consecutive scans and after 10 cycles the electrode was covered with a thick polymer film.

The extension of the cycling range to the potential of 1.1 V results in some changes in the course of the deposition curves (Fig. 2b). Namely, the relative intensity of the two oxidation peaks I_A/I_B is higher than that for deposition in the limited potential range and it increases with the number of the deposition cycles. In order to present this difference better, the

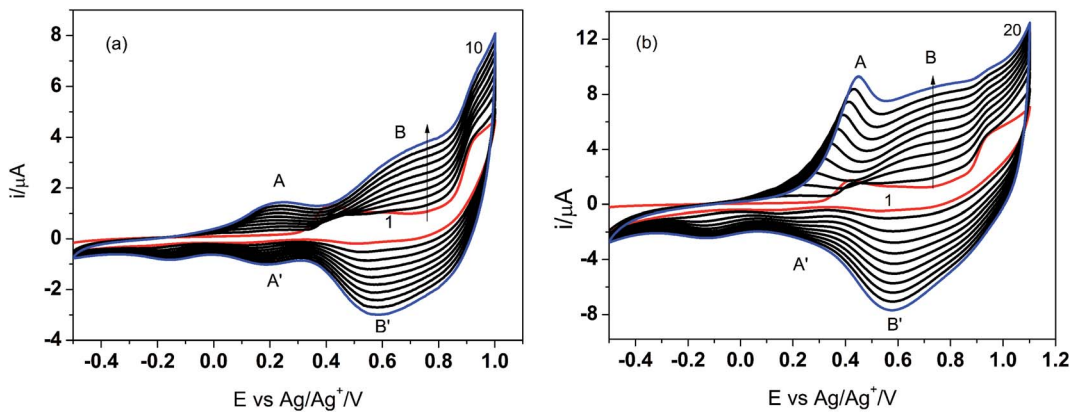

Fig. 2 Electrodeposition of poly PV-BLJ-SC9 on Pt electrode in the potential range: −0.5 → 1.0 V in 10 cycles (a) and −0.5 → 1.1 V in 20 cycles (b).

Table 1 Comparison of theoretical and experimental values of E_g and energies of HOMO–LUMO levels for PV-BLJ-SC9, PTB7 and $PC_{71}BM$

	PV-BLJ-SC9											
	trans			*cis*			PTB7[a]			$PC_{70}BM$		
Method	E_g [eV]	HOMO [eV]	LUMO [eV]	E_g [eV]	HOMO [eV]	LUMO [eV]	E_g [eV]	HOMO [eV]	LUMO [eV]	E_g [eV]	HOMO [eV]	LUMO [eV]
PBE/6-311G(d,p)	1.86	−4.83	−2.97	1.98	−4.92	−2.95	1.71	−4.40	−2.69	1.63	−5.59	−3.96
B3LYP/6-31G(d)	2.90	−5.10	−2.17	3.42	−5.55	−2.13	2.85	−4.94	−2.08	2.57	−5.63	−3.06
Cyclic voltammetry[b]	2.14	−5.20	−3.06	—	—	—	1.75	−5.44	−3.69	1.7	−5.57	−3.87
Data from literature	—	—	—	—	—	—	1.84[c]	−5.15[c]	−3.31[c]	2.0[d]	−5.90[d]	−3.90[d]

[a] Theoretical values calculated for PTB7 monomer (see ESI Fig. S2). [b] Measurements performed for mixture of *cis* and *trans* isomer. [c] Ref. 46. [d] Ossila.

number of scans in the broader potential range was increased to 20.

Moreover, the position of the peak A was shifted to more positive potentials in the consecutive cycles. This suggests that by the change of the polarization range one can modify the polymerization process and probably the structure of the polymer film. These studies will be continued to better clarify the relationship between polymerization conditions and polymer structure/properties. It would also be interesting to co-polymerize PV-BLJ-SC9 with a fullerene functionalized with a thiophene group to obtain the so-called double cable polymer–fullerene composite, which may be used as a donor–acceptor photoactive material in polymer solar cells.

The experimental values of HOMO and LUMO energies of PV-BLJ-SC9 were compared with theoretical ones calculated by two methods: PBE/6-311G(d,p) and B3LYP/6-31G(d). The model of HOMO and LUMO orbitals for PV-BLJ-SC9 is presented in Scheme 1. As shown, the electron density of HOMO level of imine is located mainly on the thiophene moieties (blue and yellow in Scheme 1) and extended to the imine bond, thiazole ring and phenylene ring. The LUMO (red and green) is located only on thiophene moieties. The LUMO–HOMO gap of PV-BLJ-SC9 was calculated to be 1.86 eV and 2.95 eV by PBE/6-311G(d,p) and B3LYP/6-31G(d) method, respectively (see Table 1).

Comparing the E_g values calculated theoretically using the B3LYP/6-31G(d) and PBE/6-311G(d,p) methods with the

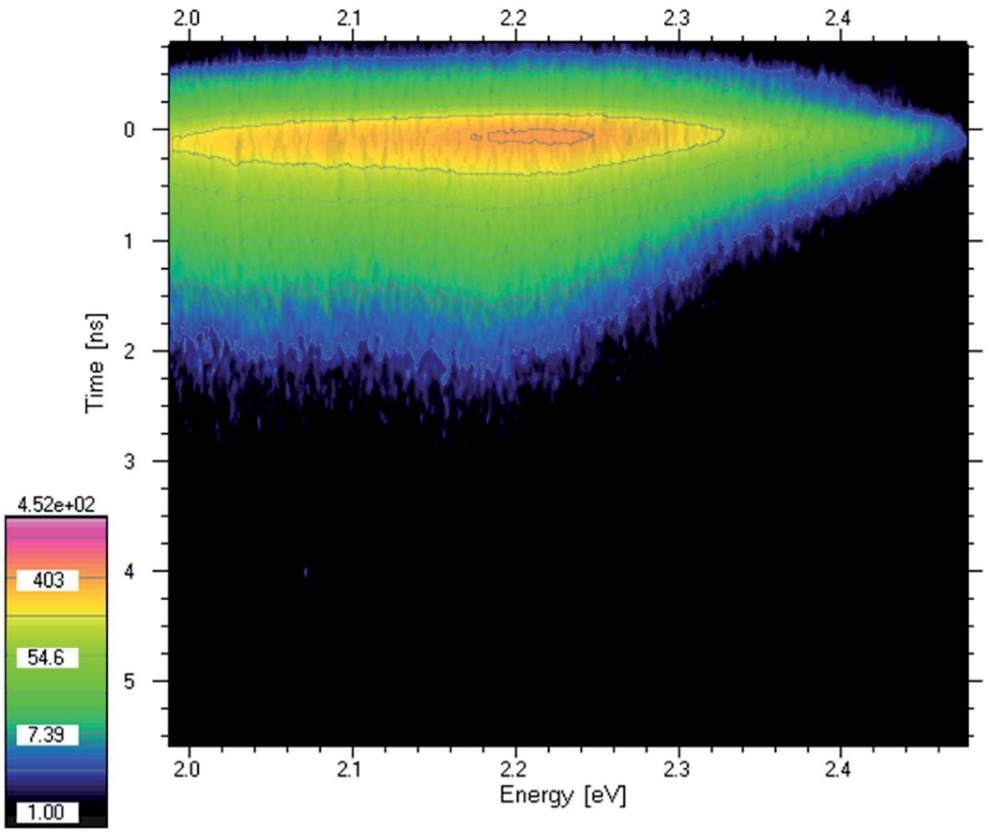

Fig. 3 Time-resolved photoluminescence spectrum of PV-BLJ-SC9 imine.

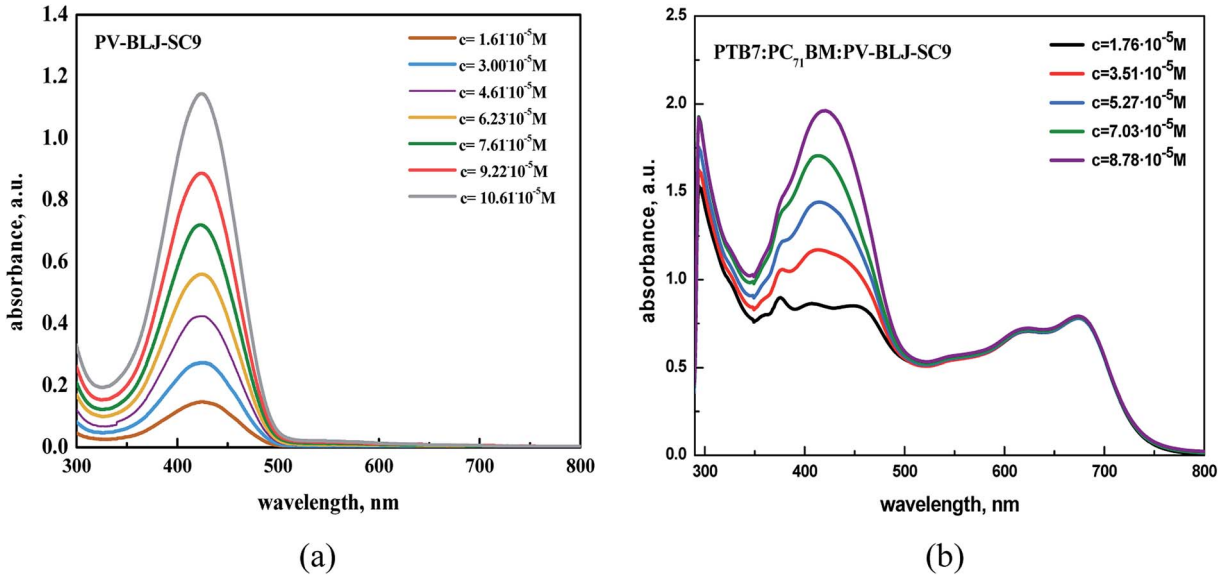

Fig. 4 UV-Vis absorption of imine (a) and PTB7:$PC_{70}BM$:imine (b) in DCB solution.

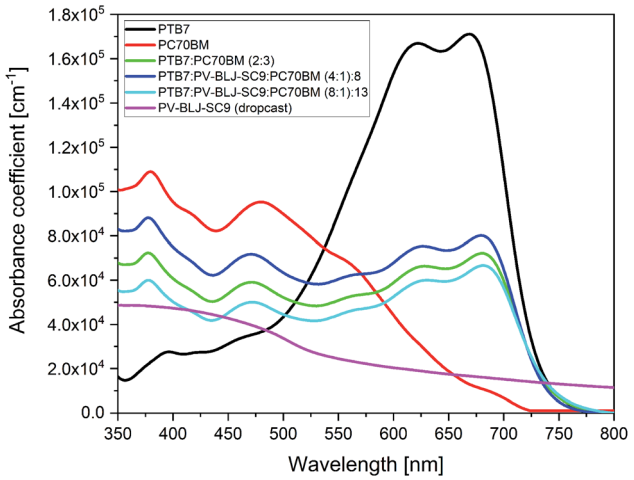

Fig. 5 The optical absorption spectra in solid layer of PV-BLJ-SC9, $PC_{70}BM$, PTB7, PTB7:$PC_{70}BM$ and ternary mixtures of (PTB7:PV-BLJ-SC9):$PC_{70}BM$ with different compositions.

experimental result obtained from the CV, it can be concluded that the latter approach better reflects the experimental result of the CV, 1.86 eV (*trans*) or 1.98 eV (*cis*) and 2.14 eV, respectively. On the other hand, a very good correlation was found between the HOMO levels determined on the basis of CV and B3LYP/6-31G(d) (−5.20 eV and −5.17 eV, respectively). It seems that in the case of the tested imine, the B3LYP and PBE functionals in conjunction with the bases used in a different way reflect the energy levels of HOMO and LUMO, *i.e.* the HOMO level is more precisely described by the B3LYP/6-31G(d) method, while the predilection of the LUMO level is better with the PBE/6-311G(d,p) approach. The problem of the selection of adequate theoretical methods for calculating the energy levels of imines needs further investigation.

3.2. Photoluminescence and time-resolved luminescence of imine

Although the photoexcited carriers in solar cells are separated and flow to different electrodes, there is always the possibility of electron–hole recombination with photon emission. The emitted photons are observed as photoluminescence (PL) and give us information about the energy difference between electron and hole states.

The spectral properties of the obtained imine were analyzed by UV-Vis absorption and photoluminescence (PL) spectroscopy. The spectra were measured from thin films (thickness ~ 1 μm) prepared by a drop cast chlorobenzene solution on copper substrate. The PL spectrum of PV-BLJ-SC9 imine together with its absorption spectrum are plotted in Fig. S3.† The PL emission was observed within the range 1.8–2.4 eV (500–700 nm), with two maxima at about 2.05 eV and 2.18 eV and a small hump at 1.9 eV. The peak at 2.05 eV and the shoulder at 1.9 eV are likely oscillatory replica of the 2.18 eV transition. The PL spectrum of imine (with peaks at about 2.18 eV to 570 nm and 2.05 eV to 605 nm) is shifted to lower energies with respect to the main peak of the absorption spectrum (at about 2.92 eV to 425 nm), which is called a Stokes shift. However, the absorption spectrum of imine also shows a weak band with a peak at about 690 nm (1.8 eV). This absorption is visible for pure imine (Fig. 4a and S3†), but its intensity increases significantly for the mixture with P7B7:$PC_{70}BM$. This low energy absorption most likely corresponds to low oscillator strength transitions, which are enhanced by intermolecular interactions.

Excitation of the sample with high energy photons (4.2 eV laser line) causes the transfer of electrons to higher excited states. Then, the electrons relax to lower excited states with the emission of light. Thus, the PL energy is lower than the excitation energy. Emission energy provides information about what energy is available after relaxation, also called the photovoltaic effect. In

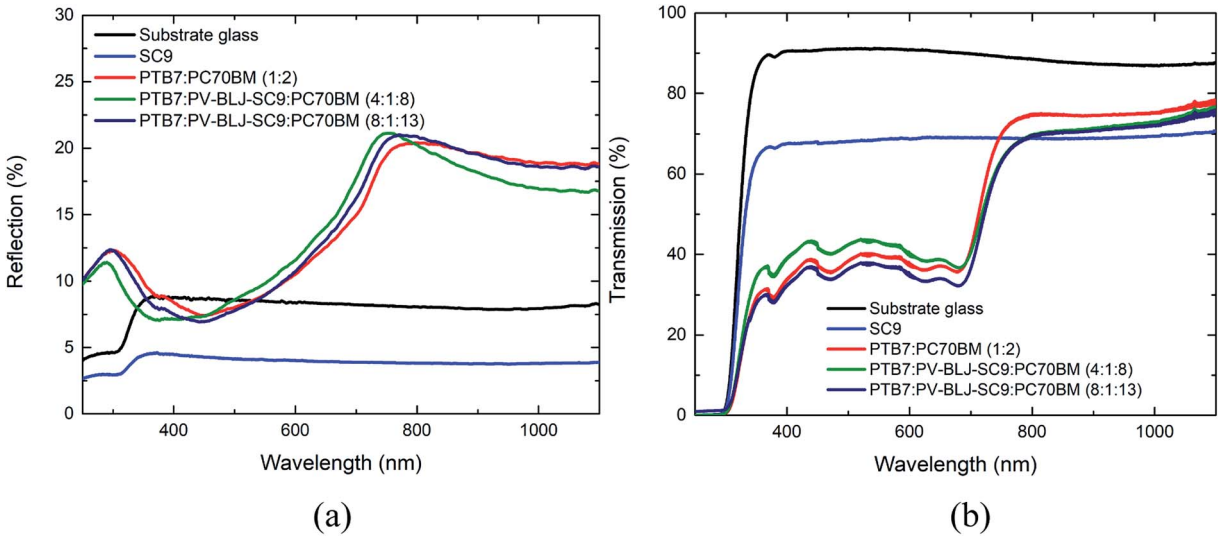

Fig. 6 Reflection (a) and transmission (b) spectra of imine and binary and ternary compositions.

Fig. 3 the time-resolved photoluminescence spectrum (TRPL) of PV-BLJ-SC9 imine is presented as a contour map. Intensity is a logarithmic scale so the intensities of the following contours are at *e*-ratio (2.72 ratio) what means that the lifetime can be directly read from the distance of the contours. The PL lifetime was about 0.3 ns. Judging from the PL intensity, this lifetime is only partially due to radiative recombination. Most of the electrons and holes are separated and recombine non-radiatively.

3.3. Absorption spectroscopy of imine, binary and ternary compositions in solution

The optical properties of imine PV-BLJ-SC9 and hybrid binary and ternary compositions based on imine:PTB7, imine:$PC_{70}BM$ and PTB7:$PC_{70}BM$:imine were investigated in dichlorobenzene (DCB) solution and in thin film by UV-Vis absorption spectroscopy. Firstly, the imine as well as binary and ternary compositions in DCB were studied by UV-Vis spectroscopy at various concentrations (see Fig. 4 and S4†). In the spectrum of PV-BLJ-SC9 imine, one can observe only one absorption band with a maximum at 424 nm, assigned to the π–π^* transition in the imine group. Its intensity linearly increases with the increase of imine concentration, according to the Beer–Lambert law.

The addition of PTB7 or $PC_{70}BM$ to imine did not influence the shape and position of the main imine absorption band (see Fig. 4b and S4†). For a mixture of imine and PTB7, one isosbestic point was found at about 500 nm, while for imine:$PC_{70}BM$:PTB7, two isosbestic points were detected at 250 and 490 nm (see Fig. S5†).

Next, the UV-Vis absorption spectra were recorded for the mixture of imine with PTB7 and $PC_{70}BM$ in proportions PTB7:$PC_{70}BM$:PV-BLJ-SC9 4 : 8 : 1 and 8 : 13 : 1 w/w/w (Fig. S6†). The same weight ratios were then used to prepare the active layers for the organic solar cell. In the spectra of PTB7 and $PC_{70}BM$, one can observe all typical signals at: 300, 621 and 680 nm, which are characteristic for PTB7 and at 358, 374, 404, 461 and 540 nm, which are typical for $PC_{70}BM$. Although the absorption ranges of PV-BLJ-SC9 and $PC_{70}BM$ overlap, the absorption maximum for imine at 424 nm is located exactly between two maxima 404 and 461 nm of the fullerene derivative.

3.4. Absorption spectroscopy of the films of imine and binary and ternary compositions

Fig. 5 presents an absorption spectrum of 1 μm thick drop cast PV-BLJ-SC9 imine, together with the spectra of spin-coated thin layers: $PC_{70}BM$, PTB7, and blends of PTB7:$PC_{70}BM$ and (PTB7:PV-BLJ-SC9):$PC_{70}BM$.

A spin-coated 100 nm layer of PV-BLJ-SC9 reveals very low absorbance, below the detection limit of the spectrometer, so it was necessary to study a thicker drop cast layer. The absorption coefficient estimated for PV-BLJ-SC9 imine was 6×10^4 cm^{-1} at its maximum (for blue and higher energy photons), whereas the absorption coefficient of the PTB7 donor material reaches 2×10^5 cm^{-1} in the visible range. The absorbance of PV-BLJ-SC9 imine starts to increase at about 1.2 eV and reaches a plateau in the range of 2.7–4.0 eV. It is probable that forbidden transitions occurring due to the oscillatory modes are responsible for the absorption with a threshold at about 1 eV, whereas allowed transitions start at the edge around 2.3 eV. This absorption band of PV-BLJ-SC9 imine is complementary to the PTB7 absorption regarding the solar spectrum, so it seems that the PV-BLJ-SC9:PTB7 mixture may be successfully used as a donor in organic solar cells instead of PTB7 alone, provided that the other properties like solubility or HOMO–LUMO energy positions of PV-BLJ-SC9 are appropriate.

The absorption of PTB7 polymer starts at about 1.6 eV and remains high up to 2.5 eV, so its spectral range is perfectly matched to the solar radiation. In the absorption spectrum of PTB7, two weakly separated maxima (at 1.8 and 2.0 eV) are observed and then above 2.5 eV, the absorption of the polymer decreases. Usually, a donor material is responsible for the absorption of solar radiation, but the $PC_{70}BM$ acceptor also

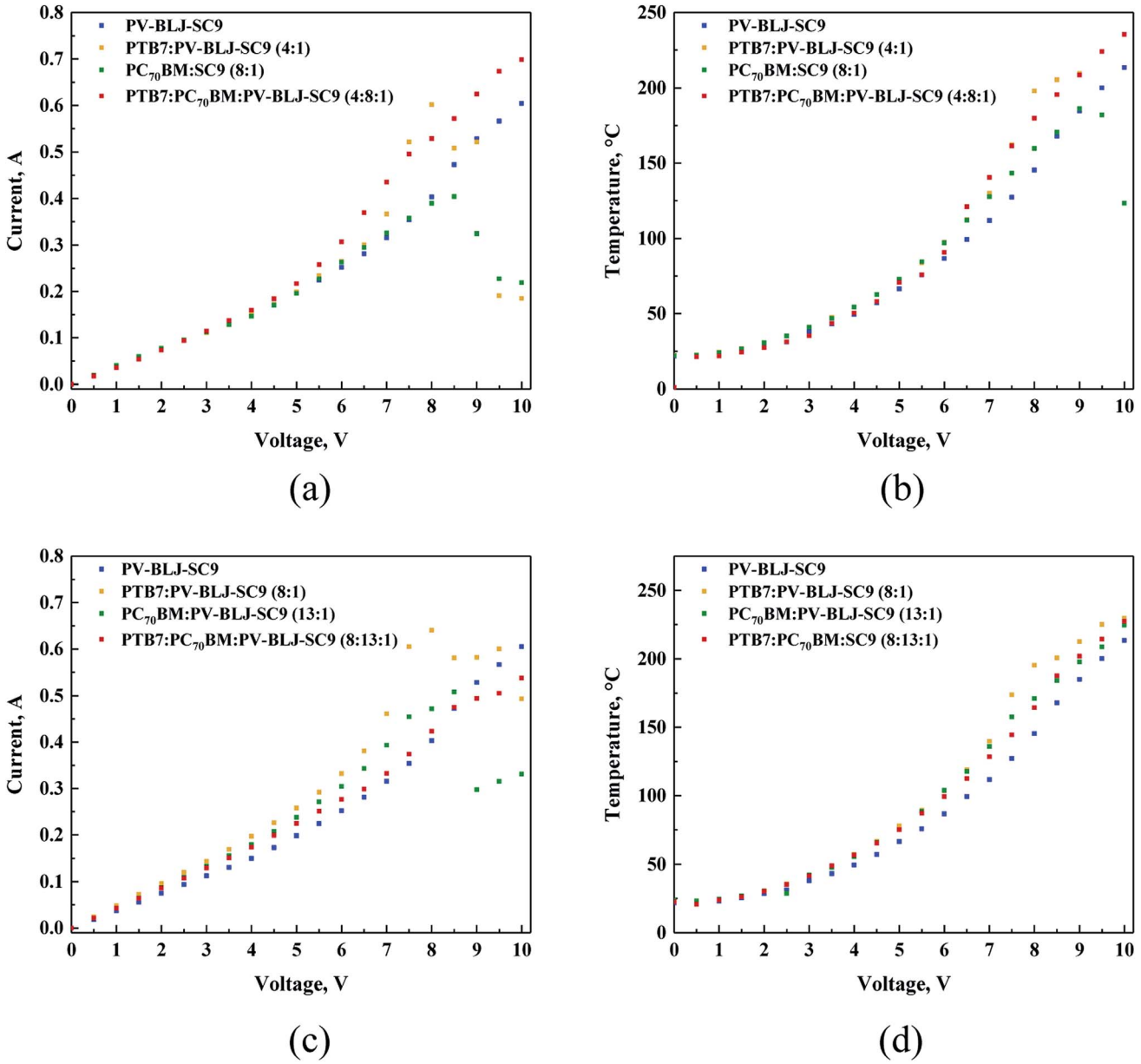

Fig. 7 The summary of thermal experiments for devices composed of PV-BLJ-SC9, PTB7:PV-BLJ-SC9 (4 : 1 and 8 : 1), $PC_{70}BM$:PV-BLJ-SC9 (8 : 1 and 13 : 1), PTB7:$PC_{70}BM$:PV-BLJ-SC9 (4 : 8 : 1 and 8 : 13 : 1): (a and c) correlation of current *versus* applied potential; (b and d) correlation of temperature *versus* applied potential.

shows significant absorption of sunlight, especially in the blue and UV range. The absorption of $PC_{70}BM$ starts at about 1.7 eV and increases up to 3.5 eV, with two characteristic broad peaks at 2.6 eV and 3.3 eV. It is noteworthy that the high absorption of $PC_{70}BM$ occurs within the range of lower PTB7 absorption. For this reason, $PC_{70}BM$ effectively complements the absorption range of PTB7 in solar cells. This can be seen in Fig. 5, where for a 2 : 3 mixture of PTB7:$PC_{70}BM$ BHJ, a broad and almost constant high absorption ranges from 1.6 eV up to 3.5 eV with four characteristic peaks, which fits well to the solar radiation spectrum. The absorption coefficient of $PC_{70}BM$ is about twice the absorption coefficient of PV-BLJ-SC9 imine in most of their absorption range.

Ternary mixtures of (PTB7:PV-BLJ-SC9):$PC_{70}BM$ with a fraction of PTB7 donor material replaced by PV-BLJ-SC9 imine did not show any additional absorption signal derived from PV-BLJ-SC9. The spectra coincided with the expected spectra for the PTB7:$PC_{70}BM$ blend with a correspondingly smaller contribution from PTB7 than in the case of the 2 : 3 mixture of PTB7:$PC_{70}BM$.

In the optical absorption spectra of binary mixtures of PTB7:PV-BLJ-SC9 and PV-BLJ-SC9:$PC_{70}BM$ (see Fig. S7†), it was not possible to observe any influence of PV-BLJ-SC9. In the absorption spectrum of PTB7:PV-BLJ-SC9, where the $PC_{70}BM$ acceptor material was replaced by PV-BLJ-SC9 imine, only a signal derived from PTB7 donor material was detected. The

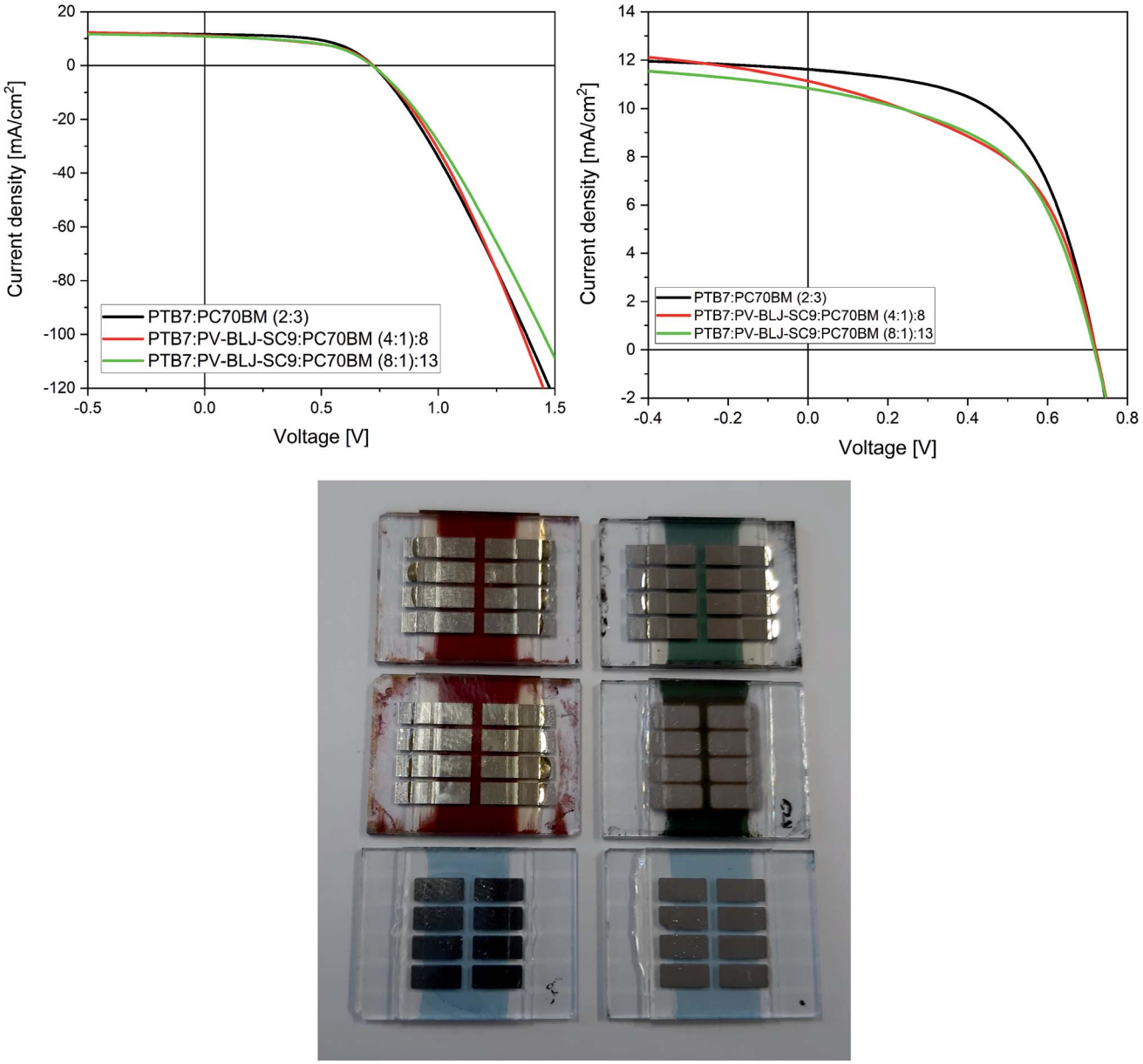

Fig. 8 J–V characteristics of PTB7:$PC_{70}BM$ solar cell (reference) and characteristics of ternary mixture (PTB7:PV-BLJ-SC9):$PC_{70}BM$ solar cells with different PV-BLJ-SC9 imine addition. The right graph is a magnification of the left one. Along with photos of the investigated devices.

signal was reduced by a factor of 2/3 compared to pure PTB7 due to the lower concentration of PTB7 in the PTB7:PV-BLJ-SC9 solution. For the PV-BLJ-SC9:$PC_{70}BM$ spectrum, where the PTB7 donor material was replaced by PV-BLJ-SC9 imine, exactly the same absorption as that for pure $PC_{70}BM$ was observed. In this case, the absolute value of absorbance is similar for both $PC_{70}BM$ and PV-BLJ-SC9:$PC_{70}BM$ layers because PV-BLJ-SC9 and $PC_{70}BM$ have relatively similar spectra (see Fig. 5).

Table 2 Photovoltaic parameters of the investigated organic solar cells with an architecture of ITO/PEDOT:PSS/active layer/In/Al with active layer based on PTB7:$PC_{70}BM$ with PV-BLJ-SC9 imine addition, under 1000 W m^{-2} illumination

Active layer	V_{oc} [V] ± 0.01	J_{SC} [mA cm^{-2}] ± 0.2	FF [%] ± 2	R_s [Ω cm^2] ± 1	R_{sh} [Ω cm^2]	PCE [%] ± 0.3
(PTB7:PV-BLJ-SC9):$PC_{70}BM$ (4 : 1) : 8	0.72/0.68[a]/0.64[b]	11.2/5.2[a]/4.9[b]	49/27[a]/27[b]	4.4	270 ± 30	4.0/1.6[a]/1.4[b]
(PTB7:PV-BLJ-SC9):$PC_{70}BM$ (8 : 1) : 13	0.72/0.68[a]/0.65[b]	10.9/5.7[a]/5.3[b]	52/28[a]/28[b]	5.7	370 ± 30	4.0/1.86[a]/1.73[b]
PTB7:$PC_{70}BM$ (2 : 3)	0.72/0.60[a]/0.60[b]	11.6/10.04[a]/9.80[b]	56/25[a]/25[b]	5.0	800 ± 80	4.7/2.3[a]/2.2[b]

[a] After 3 months. [b] After 6 months.

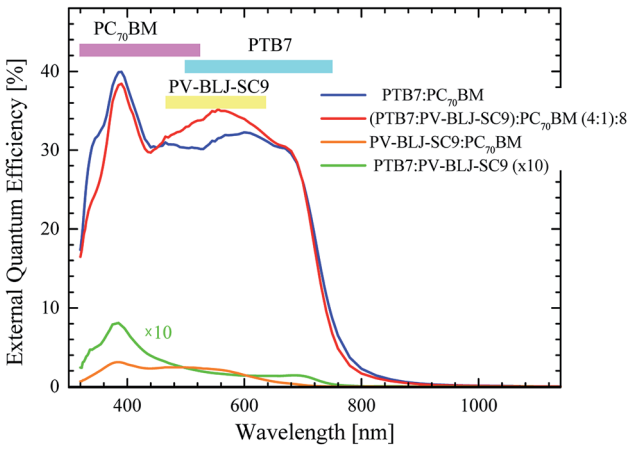

Fig. 9 EQE for solar cells with active layer of PTB7:$PC_{70}BM$ (blue curve), (PTB7:PV-BLJ-SC9):$PC_{70}BM$ with weight ratios of 4 : 1 : 8 (red curve), PV-BLJ-SC9:$PC_{70}BM$ (orange curve), and PV-BLJ-SC9:PTB7 (green curve). The absorption energy ranges of the individual components of the active layers are marked at the top of the (9).

3.5. Normal reflection and transmission of imine, binary and ternary compositions

Fig. 6a presents the normal reflection spectra for the layers of PV-BLJ-SC9 and its mixtures with PTB7 and $PC_{70}BM$, while Fig. 6b shows the transmission spectra of those films. Due to the poor adhesion of PV-BLJ-SC9 to glass, the pure imine film is very wavy, and thus the information obtained from the analysis of blue curves in Fig. 6 is only qualitative. That said, it is clear that the PV-BLJ-SC9 film has significantly lower reflection and lower transmission than the pure substrate glass in the whole investigated wavelength range. Moreover, the drop in both reflection and transmission values is almost uniform at wavelengths greater than 400 nm. As such, the addition of PV-BLJ-SC9 to already existing polymer-fullerene mixtures to form the active layer of organic solar cells gives hope for increasing the absorption coefficients of the active layers, particularly in spectral regions where the absorption coefficient is low. Indeed, the transmission coefficient of PTB7:PV-BLJ-SC9:$PC_{70}BM$ mixtures – depicted by green and purple curves in Fig. 6 – is lower than that of PTB7:$PC_{70}BM$ mixtures without the imine addition (red curves), for wavelengths above 800 nm, for which the absorption coefficient of the PTB7:$PC_{70}BM$ blend is generally low. Moreover, the reflection coefficient of PTB7:PV-BLJ-SC9:$PC_{70}BM$ mixtures in this wavelength range did not increase – it either decreased (for the 4 : 1 : 8 ratio) or remained similar (for the 8 : 1 : 13 ratio). Thus, we conclude that the absorption of PTB7:PV-BLJ-SC9:$PC_{70}BM$ mixtures at wavelengths above 800 nm is greater than without the PV-BLJ-SC9 addition. This gives hope for increasing the efficiency of the PTB7:$PC_{70}BM$-based solar cells.

Analysis of the spectra at wavelengths below 800 nm is more problematic. Depending on the specific mass ratio, the transmission values for the PTB7:PV-BLJ-SC9:$PC_{70}BM$ films at the 400–700 nm range are either above (4 : 1 : 8) or below (8 : 1 : 13) the values for the PTB7:$PC_{70}BM$ film. Similarly, at 400–700 nm the reflection coefficient for the 4 : 1 : 8 PTB7:PV-BLJ-SC9:$PC_{70}BM$ film is higher than that for the 8 : 1 : 13 ratio, as well as for the PTB7:$PC_{70}BM$ film without PV-BLJ-SC9. This suggests that the absorption of the 8 : 1 : 13 blend is higher in this spectral region than for the 4 : 1 : 8 blend. This may have many causes, one of which is the low adhesion of PV-BLJ-SC9 to glass. Due to the repelling forces of imine and glass substrate, at high concentrations of PV-BLJ-SC9, the spin-cast films might be less dense, and thus, optically thinner. At wavelengths below 400 nm, the reflection coefficient of the 4 : 1 : 8 blend is lower than that of the 8 : 1 : 13 blend, but since this is the spectral region in which glass absorbs light itself, the difference in this range can be neglected. Thus, from the optical standpoint it can be concluded that the 8 : 1 : 13 blend is closer to optimum.

3.6. Thermal imaging

In the next step of our work, we investigated the thermal behaviour of devices based on PV-BLJ-SC9 imine. The thermal behaviour was recorded for the devices of a general configuration: ITO/active layer/Ag/ITO, with different active layers: PV-BLJ-SC9, PTB7:PV-BLJ-SC9 (4 : 1 and 8 : 1), $PC_{70}BM$:PV-BLJ-SC9 (8 : 1 and 13 : 1), and PTB7:$PC_{70}BM$:PV-BLJ-SC9 (4 : 8 : 1 and 8 : 13 : 1). The weight ratios of the components were the same as in the active layers used in solar cells.

The *I–V* plots presented in Fig. 7a and c can be divided into approximately three regions: 0–5 V, 5–8.5 V and above 8.5 V, of different slopes. The resistance values obtained from these slopes range from 23.3 to 18.5 Ω. Thus, all organic layers, regardless of their composition, do not behave as expected, as a typical ohmic conductor. Namely, the resistivity of PV-BLJ-SC9 and the compositions containing this imine, decrease with the increasing voltage. The non-linear lines through the beginning of the graph are rather similar to the typical behaviour of an electrolyte.

It is interesting to note that for all studied samples the current increased in the same linear fashion up to 5 V. Afterwards, the curves diverge giving different current values, where the highest conductivity corresponds to the layer composed of PTB7:$PC_{70}BM$:PV-BLJ-SC9 (4 : 8 : 1 ratio). Moreover, two component mixtures showed unstable behaviour above 8.5 V. This might be related to degradation of the samples. The thermal behaviour under the applied voltage was recorded for all active layers mentioned above.

Analysing the thermal outputs (Fig. 7b and d) one can notice that the temperature of the active layer increases in the function of applied voltage in a similar way as the current *vs.* voltage. In case of samples displaying decline of current flow, a decline of temperature was also observed. The three-component layer showed the highest heat resistance reaching a value above 225 °C, at the potential of 10 V.

The detailed examination of thermal images showed very similar behaviour in the tested devices: at the beginning, the heating was relatively homogeneous with the overheating zone close to the positive electrode (left-hand side in the images). Upon the temperature increase, the difference becomes more evident

due to different heat distribution. The overheating zone is located always at the positive electrode, as can be seen in Fig. S8 and S9.†

Finally, a comparison of the curves in Fig. 7a and c with those in Fig. 7b and d was performed to determine whether the amount of imine contained in the two-component PTB7:PV-BLJ-SC9 (4 : 1 and 8 : 1), $PC_{70}BM$:PV-BLJ-SC9 (8 : 1 and 13 : 1) and three-component PTB7:$PC_{70}BM$:PV-BLJ-SC9 (4 : 8 : 1 and 8 : 13 : 1) active layers influences the performance of the device.

First, it was found that regardless of the active layer composition, the current increased in the same linear fashion up to 5 V with some deviation. On the other hand, the conductivity of the samples changed consistently as follows, in order of decreasing current values: PTB7:PV-BLJ-SC9 (8 : 1) > $PC_{70}BM$:PV-BLJ-SC9 (13 : 1) > PTB7:$PC_{70}BM$:PV-BLJ-SC9 (8 : 13 : 1). Above 5 V, the two-component samples displayed higher currents compared to the imine and three-component sample. Also, in these cases, above 7.5 V the samples PTB7:PV-BLJ-SC9 and $PC_{70}BM$:PV-BLJ-SC9 revealed instability but with smaller current decrease. These phenomena might suggest that some reaction may occur in the organic layer. It could also be due to the highest heat resistance of the sample PTB7:$PC_{70}BM$:PV-BLJ-SC9 (8 : 13 : 1) at the high potential of 10 V, as reported above.

In summary, the results of thermal experiments together with current recording at increasing potential clearly indicate that the presence of PV-BLJ-SC9 in the mixture has a beneficial impact in terms of current flow stability at temperatures above 200 °C, compared to two-component layers with the same imine as an additive.

3.7. Preliminary investigations of photovoltaic activity of imine

Finally, the imine PV-BLJ-SC9 was tested as a component of active layer in the bulk-heterojunction organic solar cells. Current–voltage characteristics of organic solar cells containing PV-BLJ-SC9 imine in their active layers of different compositions are presented in Fig. 8 and S10.†

The *J–V* measurements of solar cells with ternary blends of (PTB7:PV-BLJ-SC9):$PC_{70}BM$ showed that the highest power conversion efficiency (PCE) of 4.7% was achieved for the reference cell without the addition of PV-BLJ-SC9 imine (see Fig. 8 and Table 2). For the solar cells with a part of PTB7 donor material replaced by PV-BLJ-SC9 imine, the reduction of efficiency by 15% to PCE = 4.0% was observed. The decrease of efficiency was associated with a 10% decrease in the fill factor and a small decrease of short circuit current density, while the open circuit voltage remained almost unchanged. Current density is proportional to the concentration of photocarriers, so its decrease for (PTB7:PV-BLJ-SC9):$PC_{70}BM$-based solar cells was due to the lower absorption of photons after partial replacement of the PTB7 donor material by PV-BLJ-SC9 imine, because of the low absorption coefficient of the imine in the visible range. The fill factor depends on series and shunt resistances and BHJ microscopic structure. Both resistances are introduced in an equivalent circuit of a non-ideal solar cell. From the change of *J–V* slope for low voltages (see Fig. 8), it is evident that the addition of PV-BLJ-SC9 imine leads to a decrease in the shunt resistance. The shunt resistance, obtained from the fitting of *J–V* curves using a model of a non-ideal solar cell, was up to 3 times smaller for the cells with PV-BLJ-SC9 imine. This and lower FF suggested that poorly soluble imine deteriorated the BHJ microscopic structure of the PTB7:$PC_{70}BM$ blend. For all solar cells, the open circuit voltage remained constant due to the same active donor and acceptor, which was only slightly changed by the presence of PV-BLJ-SC9 imine. The value of open circuit voltage depends mainly on the difference between acceptor LUMO and donor HOMO energy levels, and therefore its value is characteristic for a given cell composition.

To check the lifetime of constructed organic solar cells based on PTB7:$PC_{70}BM$:imine, the devices were tested again after approximately 3 and 6 months (see Table 2). The encapsulated devices were kept in air atmosphere with a small influx of sunlight. For all investigated devices, the decreases in photovoltaic parameters were observed after 3 months, but then, in a longer time scale (6 months) the parameters nearly stabilized (see Table 2). The current–voltage characteristics of the organic solar cells with and without PV-BLJ-SC9 imine in their active layers of different compositions, investigated after 3 and 6 months, are presented in Fig. S11.† Additionally, we did not observe substantial differences in the photovoltaic parameters of all imine-containing pixels of the solar cell (8 pixels for each device), measured immediately after construction, after 3 months and after 6 months (see Fig. S12†). In contrast, more fluctuations were found for the pixels of the reference device (see Fig. S12†).

3.8. Photo-electric spectroscopy

Photocurrent spectra of active layers of PTB7:$PC_{70}BM$, (PTB7:PV-BLJ-SC9):$PC_{70}BM$ with weight ratios of (4 : 1) : 8, PV-BLJ-SC9:$PC_{70}BM$, and PTB7:PV-BLJ-SC9 were measured. Then, the external quantum efficiency (EQE) spectra were determined and plotted in Fig. 9. The EQE values were calculated as the ratio of the photocurrent (converted to an electron flux) to the incident photon flux.

The upper bars in Fig. 9 mark the absorption energy ranges corresponding to individual components of the active layers. The signal originating from PTB7 starts at about 1.6 eV and reaches its maximum at 2 eV. $PC_{70}BM$ is responsible for the signal in the range of 3.0–3.8 eV, whereas PV-BLJ-SC9 imine acts in the range of 1.8–3 eV. A comparison of EQE spectra of (PTB7:PV-BLJ-SC9):$PC_{70}BM$ and PTB7:$PC_{70}BM$ indicates that the extra photocurrent recorded in the energy range of 1.8–2.8 eV with a maximum at about 2.3 eV is due to the presence of PV-BLJ-SC9 imine. In contrast, the EQE for the cells based on PV-BLJ-SC9:$PC_{70}BM$ and PV-BLJ-SC9:PTB7 cells were very small, especially that for PV-BLJ-SC9:PTB7. The EQE for the latter cell started to increase at about 1.6 eV, and reached a small peak at 3.3 eV as for the cell with PTB7 donor. The EQE results are in accordance with the J_{SC} values from the *J–V* measurements. The EQE for PTB7:$PC_{70}BM$ with the addition of PV-BLJ-SC9 imine shows some improved performance in the 1.8–2.0 eV energy range, evidently due to the presence of imine, but there is a decrease in the number of created photocarriers for higher energies.

4. Conclusions

In conclusion, this work was focused on the investigations of a new unsymmetrical imine with four thiophene rings being a mixture of *cis* and *trans* isomers and its binary and ternary compositions toward optoelectronics and photonics. We studied relationships between the imine and PTB7 or $PC_{70}BM$ and their selected properties crucial for applications. It was found that imine exhibited photoluminescence in a thin film with two maxima at about 2.05 eV and 2.18 eV. Excitation of the imine at the 4.2 eV laser line causes the transfer of electrons to higher excited states, and then the electrons relax to lower excited states, and then recombine from these states reaching ground state with the emission of light. The time-resolved photoluminescence experiment indicated that the photoluminescence lifetime of imine is about 0.3 ns. The absorption coefficient of imine was found to be about 6×10^4 cm^{-1}. The LUMO and HOMO energies of the imine determined from the cyclic voltammogram in DCM solution were about −3.06 eV and −5.20 eV, respectively. The band gap energy (E_g) of the imine was about 2.14 eV. The LUMO–HOMO gap of *cis*- and *trans*-PV-BLJ-SC9 was calculated by PBE/6-311G(d,p) and B3LYP/6-31G(d) methods to find the best one for imine characterization. Theoretical results obtained by B3LYP/6-31G(d) method are in quite good correlation with the experimental data. PTB7 in association with the imine modifies the electronic spectrum of composition, however, the imine absorption band was not affected by PTB7. In the PTB7:imine composition, three main absorption bands were found at 424 nm, 625 nm and 670 nm. $PC_{70}BM$ does not introduce substantial changes in the absorption spectrum of the composition with the imine. Some changes were found at about 370 nm that were dependent on the concentration of the $PC_{70}BM$:imine composition. Organic solar cells with the imine in the active layer based on PTB7:$PC_{70}BM$ exhibited a PCE of about 4% and EQE of about 40% at photon energy 3.3 eV. The presence of the imine in the ternary composition has a beneficial impact in terms of current flow stability at temperatures above 200 °C, compared to two-component layers with the same imine as an additive.

Finally, the synthesized imine can be considered in the future as a compound for further modification of the active organic solar cell material by co-polymerization with thiophene-modified fullerene to obtain the so-called double cable polymer–fullerene composite, which may be used as a donor–acceptor photoactive material in polymer solar cells.

Author contributions

Beata Jewloszewicz: investigation, Krzysztof Artur Bogdanowicz: investigation, Wojciech Przybyl: investigation, Karolina Dysz: investigation, Agnieszka Dylong: investigation, Agnieszka Gonciarz: investigation, Robert Pich: investigation, Wojciech Mech: investigation, Krzysztof P. Korona: investigation, analyses, Maria Kaminska: reviewing and editing, Kamila Zarębska: investigation, Magdalena Skompska: investigation, reviewing and editing, Andrzej Kaim: investigation, Arkadiusz Ciesielski: investigation, analyses, Agnieszka Iwan: writing-original draft preparation, supervision, writing-reviewing and editing, conceptualization.

Conflicts of interest

All authors have read and agreed to the published version of the manuscript.

Acknowledgements

Authors are grateful for financial support from Polish National Centre of Research and Development (TECHMATSTRATEG1/347431/14/NCBR/2018). The theoretical results presented in this work were obtained with the computational resources of the Interdisciplinary Center for Mathematical and Computational Modeling at Warsaw University (Grant G15-11).

References

1 M. A. Green, K. Emery, Y. Hishikawa, W. Warta and E. D. Dunlo, Solar cell efficiency tables (version 42), *Prog. Photovoltaics Res. Appl.*, 2013, **21**, 827–837.
2 K. D. G. I. Jayawardena, L. J. Rozanski, C. A. Mills, M. J. Beliatis, N. A. Nismy and S. R. P. Silva, 'Inorganics-in-Organics': recent developments and outlook for 4G polymer solar cells, *Nanoscale*, 2013, **5**, 8411–8427.
3 E. Bundgaard and F. C. Krebs, Low band gap polymers for organic photovoltaics, *Sol. Energy Mater. Sol. Cells*, 2007, **91**, 954–985.
4 X. Zhan and D. Zhu, Conjugated polymers for high-efficiency organic photovoltaics, *Polym. Chem.*, 2010, **1**, 409–419.
5 M. Palewicz and A. Iwan, Photovoltaic Phenomenon in Polymeric Thin Layer Solar Cells, *Curr. Phys. Chem.*, 2011, **1**, 27–54.
6 Q. Lin, H. Huang, Y. Jing, H. Fu, P. Chang, D. Li, Y. Yao and Z. Fan, Flexible photovoltaic technologies, *J. Mater. Chem. C*, 2014, **2**, 1233–1247.
7 T. Ameri, P. Khoram, J. Min and C. J. Brabec, Organic ternary solar cells: a review, *Adv. Mater.*, 2013, **25**, 4245–4266.
8 M. S. Ryu, H. J. Cha and J. Jang, Improvement of operation lifetime for conjugated polymer:fullerene organic solar cells by introducing a UV absorbing film, *Sol. Energy Mater. Sol. Cells*, 2010, **94**, 152–156.
9 M. O. Reese, S. A. Gevorgyan, M. Jørgensen, E. Bundgaard, S. R. Kurtz, D. S. Ginley, D. C. Olson, M. T. Lloyd, P. Morvillo, E. A. Katz, A. Elschner, O. Haillant, T. R. Currier, V. Shrotriya, M. Hermenau, M. Riede, K. R. Kirov, G. Trimmel, T. Rath, O. Inganas, F. Zhang, M. Andersson, K. Tvingstedt, M. Lira-Cantu, D. Laird, C. McGuiness, S. Gowrisanker, M. Pannone, M. Xiao, J. Hauch, R. Steim, D. M. DeLongchamp, R. Rosch, H. Hoppe, N. Espinosa, A. Urbina, G. Yaman-Uzunoglu, J.-B. Bonekamp, A. J. J. M. van Breemen, C. Girotto, E. Voroshazi and F. C. Krebs, Consensus stability testing protocols for organic photovoltaic materials and devices, *Sol. Energy Mater. Sol. Cells*, 2011, **95**, 1253–1267.

10 A. Iwan and A. Chuchmała, Perspectives of applied graphene: polymer solar cells, *Prog. Polym. Sci.*, 2012, **37**, 1805–1828.

11 Y. Li, Molecular design of photovoltaic materials for polymer solar cells: towards suitable electronic energy levels and broad absorption, *Acc. Chem. Res.*, 2012, **45**, 723–733.

12 J. Kesters, S. Kudret, S. Bertho, N. van den Brande, M. Defour, B. van Mele, H. Penxten, L. Lutsen, J. Manca, D. Vanderzande and W. Maes, Enhanced intrinsic stability of the bulk heterojunction active layer blend of polymer solar cells by varying the polymer side chain pattern, *Org. Electron.*, 2014, **15**, 549–562.

13 J. T. Chen and C. S. Hsu, Conjugated polymer nanostructures for organic solar cell applications, *Polym. Chem.*, 2011, **2**, 2707–2722.

14 G. Sauve and R. Fernando, Beyond Fullerenes: Designing Alternative Molecular Electron Acceptors for Solution-Processable Bulk Heterojunction Organic Photovoltaics, *J. Phys. Chem. Lett.*, 2015, **6**, 3770–3780.

15 Y.-Y. Lai, Y.-J. Cheng and C. S. Hsu, Applications of functional fullerene materials in polymer solar cells, *Energy Environ. Sci.*, 2014, **7**, 1866–1883.

16 A. Iwan and D. Sek, Processible polyazomethines and polyketanils: from aerospace to light emitting diodes and other advanced applications, *Prog. Polym. Sci.*, 2008, **33**, 289–345.

17 A. Iwan and D. Sek, Polymers with triphenylamine units: photonic and electroactive materials, *Prog. Polym. Sci.*, 2011, **36**, 1277–1325.

18 A. W. Jeevadason, K. K. Murugavel and M. A. Neelakantan, Review on Schiff bases and their metal complexes as organic photovoltaic materials, *Renewable Sustainable Energy Rev.*, 2014, **36**, 220–227.

19 A. Iwan, M. Palewicz, M. Krompiec, M. Grucela-Zajac, E. Schab-Balcerzak and A. Sikora, Synthesis, materials characterization and opto(electrical) properties of unsymmetrical azomethines with benzothiazole core, *Spectrochim. Acta, Part A*, 2012, **97**, 546–555.

20 A. Iwan, An overview of LC polyazomethines with aliphatic–aromatic moieties: thermal, optical, electrical and photovoltaic properties, *Renewable Sustainable Energy Rev.*, 2015, **52**, 65–79.

21 S. Barik, T. Bletzacker and W. G. Skene, π-Conjugated fluorescent azomethine copolymers: opto-electronic, halochromic, and doping properties, *Macromolecules*, 2012, **45**, 1165–1173.

22 A. Iwan, P. Bilski and M. Kłosowski, Thermoluminescence measurements of liquid crystal azomethines and poly(azomethine)s with different shape as thermodetectors, *J. Lumin.*, 2010, **130**, 2362–2367.

23 A. Gonciarz, R. Pich, K. A. Bogdanowicz, B. Jewloszewicz, W. Przybył, K. Dysz, A. Dylong, A. Kwak, A. Kaim, A. Iwan, J. Rusin and A. Januszko, UV-Vis Absorption Properties of New Aromatic Imines and Their Compositions with Poly({4,8-bis[(2-Ethylhexyl)oxy]Benzo[1,2-b:4,5-b′] Dithiophene-2,6-diyl}{3-Fluoro-2-[(2-Ethylhexyl)Carbonyl] Thieno[3,4-b]Thiophenediyl}), *Materials*, 2019, **12**, 4191.

24 H. Wen, H. Niu, B. Li, X. Ma, X. Bai, Y. Zhang and W. Wang, Synthesis and acidochromic, electrochromic properties of Schiff bases containing furan and triphenylamine units, *Synth. Met.*, 2015, **202**, 89–97.

25 X. Wu, W. Wang, B. Li, Y. Hou, H. Niu, Y. Zhang, S. Wang and X. Bai, Synthesis and electrochromic, acidochromic properties of Schiff bases containing triphenylamine and thiophene units, *Spectrochim. Acta, Part A*, 2015, **140**, 398–406.

26 K. A. Bogdanowicz, B. Jewłoszewicz, A. Iwan, K. Dysz, W. Przybyl, A. Januszko, M. Marzec, K. Cichy, K. Świerczek, L. Kavan, M. Zukalová, V. Nadazdy, R. Subair, E. Majkova, M. Micusik, M. Omastova, M. D. Özeren, K. Kamarás, D. Y. Heo and S. Y. Kim, Selected Electrochemical Properties of 4,4'-((1E,1'E)-((1,2,4-thiadiazole-3,5-diyl) bis(azaneylylidene))bis(methaneylylidene))bis(N,N-di-p-tolylaniline) towards Perovskite Solar Cells with 14.4% Efficiency, *Materials*, 2020, **13**, 2440.

27 M. L. Petrus, T. Bein, T. Dingemans and P. Docampo, A low cost azomethine-based hole transporting material for perovskite photovoltaics, *J. Mater. Chem. A*, 2015, **3**, 12159–12162.

28 A. W. Jeevadason, K. K. Murugavel and M. A. Neelakantan, Review on Schiff bases and their metal complexes as organic photovoltaic materials, *Renewable Sustainable Energy Rev.*, 2014, **36**, 220–227.

29 M. L. Petrus, R. K. M. Bouwer, U. Lafont, S. Athanasopoulos, N. C. Greenham and T. J. Dingemans, Small-molecule azomethines: organic photovoltaics via Schiff base condensation chemistry, *J. Mater. Chem. A*, 2014, **2**, 9474–9477.

30 N. Y. Canli, M. Safak-Boroglu, B. Bilgin-Eran and S. Gunes, Bilayer polymer/fullerene solar cells with a liquid crystal, *Thin Solid Films*, 2014, **560**, 71–76.

31 C. Moussalem, O. Segut, F. Gohier, M. Allain and P. Frere, Facile Access via Green Procedures to a Material with the Benzodifuran Moiety for Organic Photovoltaics, *ACS Sustainable Chem. Eng.*, 2014, **2**, 1043–1048.

32 Q. Tan, X. Zhang, L. Mao, G. Xin and S. Zhang, Novel zinc porphyrin sensitizers for dye-sensitized solar cells: synthesis and spectral, electrochemical, and photovoltaic properties, *J. Mol. Struct.*, 2013, **1035**, 400–406.

33 M. L. Petrus, F. S. F. Morgenstern, A. Sadhanala, R. H. Friend, N. C. Greenham and T. J. Dingemans, Device Performance of Small-Molecule Azomethine-Based Bulk Heterojunction Solar Cells, *Chem. Mater.*, 2015, **27**, 2990–2997.

34 M. Grucela-Zajac, K. Bijak, S. Kula, M. Filapek, M. Wiacek, H. Janeczek, L. Skorka, J. Gasiorowski, K. Hingerl, N. S. Sariciftci, N. Nosidlak, G. Lewinska, J. Sanetra and E. Schab-Balcerzak, (Photo)physical Properties of New Molecular Glasses End-Capped with Thiophene Rings Composed of Diimide and Imine Units, *J. Phys. Chem. C*, 2014, **118**, 13070–13086.

35 D. Sek, M. Siwy, B. Bijak, M. Filapek, G. Malecki, E. M. Nowak, J. Sanetra, A. Jarczyk-Jedryk, K. Laba, M. Lapkowski and E. Schab-Balcerzak, Optical and

electrochemical properties of novel thermally stable Schiff bases bearing naphthalene unit, *J. Electroanal. Chem.*, 2015, **751**, 128–136.

36 D. Sek, M. Siwy, G. Malecki, S. Kotowicz, S. Golba, E. M. Nowak, J. Sanetra and E. Schab-Balcerzak, Polycyclic aromatic hydrocarbons connected with Schiff base linkers: experimental and theoretical photophysical characterization and electrochemical properties, *Spectrochim. Acta, Part A*, 2017, **175**, 168–176.

37 T. Ameri, P. Khoram, J. Min and C. J. Brabec, Organic Ternary Solar Cells: A Review, *Adv. Mater.*, 2013, **25**, 4245–4266.

38 E. M. Nowak, J. Sanetra, M. Grucela and E. Schab-Balcerzak, Azomethine naphthalene diimides as component of active layers in bulk heterojunction solar cells, *Mater. Lett.*, 2015, **157**, 93–98.

39 K. A. Bogdanowicz, B. Jewloszewicz, K. Dysz, W. Przybyl, A. Dylong, W. Mech, K. P. Korona, M. Skompska, A. Kaim, M. Kamińska and A. Iwan, Electrochemical and optical studies of new symmetrical and unsymmetrical imines with thiazole and thiophene moieties, *Electrochim. Acta*, 2020, **332**, 135476.

40 M. J. Frisch; G. W. Trucks; H. B. Schlegel; G. E. Scuseria; M. A. Robb; J. R. Cheeseman; G. Scalmani; V. Barone; G. A. Petersson; H. Nakatsuji; X. Li; M. Caricato; A. V. Marenich; J. Bloino; B. G. Janesko; R. Gomperts; B. Mennucci; H. P. Hratchian; J. V. Ortiz; A. F. Izmaylov; J. L. Sonnenberg; D. Williams-Young; F. Ding; F. Lipparini; F. Egidi; J. Goings; B. Peng; A. Petrone; T. Henderson; D. Ranasinghe; V. G. Zakrzewski; J. Gao; N. Rega; G. Zheng; W. Liang; M. Hada; M. Ehara; K. Toyota; R. Fukuda; J. Hasegawa; M. Ishida; T. Nakajima; Y. Honda; O. Kitao; H. Nakai; T. Vreven; K. Throssell; J. A. Montgomery Jr; J. E. Peralta; F. Ogliaro; M. J. Bearpark; J. J. Heyd; E. N. Brothers; K. N. Kudin; V. N. Staroverov; T. A. Keith; R. Kobayashi; J. Normand; K. Raghavachari; A. P. Rendell; J. C. Burant; S. S. Iyengar; J. Tomasi; M. Cossi; J. M. Millam; M. Klene; C. Adamo; R. Cammi; J. W. Ochterski; R. L. Martin; K. Morokuma; O. Farkas; J. B. Foresman and D. J. Fox, *Gaussian 16, Revision A. 03*, Gaussian, Inc., Wallingford CT, 2016.

41 W. Kohn and L. J. Sham, Self-Consistent Equations Including Exchange and Correlation Effects, *Phys. Rev.*, 1965, **140**, A1133–A1138.

42 A. D. Becke, Density-functional exchange-energy approximation with correct asymptotic behavior, *Phys. Rev.*, 1988, **38**, 3098–3100.

43 C. Lee, W. Yang and R. G. Parr, Development of the Colle-Salvetti correlation-energy formula into a functional of the electron density, *Phys. Rev. B: Condens. Matter Mater. Phys.*, 1988, **37**, 785–789.

44 J. P. Perdew, K. Burke and M. Ernzerhof, Generalized Gradient Approximation Made Simple, *Phys. Rev. Lett.*, 1996, **77**, 3865–3868.

45 A. Różycka, K. A. Bogdanowicz, N. Górska, J. Rysz, M. Marzec, A. Iwan, R. Pich and A. Januszko, Influence of TiO_2 nanoparticles on liquid crystalline, structural and electrochemical properties of (8z)-n-(4-((z)-(4-pentylphenylimino)methyl)benzylidene)-4-pentylbenzenamine, *Materials*, 2019, **12**, 1097.

46 C. Gu, Z. Zhang, S. Sun, Y. Pan, C. Zhong, Y. Lv, M. Li, K. Ariga, F. Huang and Y. Ma, In Situ Electrochemical Deposition and Doping of C 60 Films Applied to High-Performance Inverted Organic Photovoltaics, *Adv. Mater.*, 2012, **24**, 5727–5731.

